Int. J. Electrochem. Sci., 10 **(2015)** 2825 - 2838

International Journal of
ELECTROCHEMICAL
SCIENCE
www.electrochemsci.org

Cyclic Voltammetry for Synthesizing Carbon Supported Pt-Cu Alloy with Superior Oxygen Reduction Activity

Youqin Lu[1,3], *Min Wang*[2], *Cunguang Yuan*[3], *Jinsheng Zhao*[1,*], *Jianfeng Yu*[3,*]

[1]Shandong Key Laboratory of Chemical Energy Storage and Novel Cell Technology, Liaocheng University, Liaocheng, 252059, P. R. China
[2]Liaocheng Hospital, Liaocheng, 252000, Shandong Province, P. R. China
[3]College of Science, China University of Petroleum (East China), Qingdao, 266580, P. R. China
[*]E-mail: j.s.zhao@163.com; yujf@upc.edu.cn

Received: 23 December 2014 / *Accepted:* 29 January 2015 / *Published:* 24 February 2015

Cyclic voltammetry (CV) was used to fabricate carbon supported Pt-Cu alloy (Pt-Cu/C) for oxygen reduction reaction (ORR) at ambient temperature. A flowerlike structure of Pt-Cu nanoparticles were analyzed by scanning electron microscopy and X-ray photoelectron spectroscopy was used to confirm the surface chemical composition and metallic state. And, electrochemical measurements such as CV, rotating disk electrode, rotating ring-disk and electrochemical impedance spectroscopy were applied to obtain the kinetic constants and the reaction mechanisms of the ORR. Compared with Pt/C, Cu/C, Pt-Cu/C exhibits the highest efficient catalytic activity for ORR, as evidenced by the highest current densities of the polarization curves, lowest onset oxidation potential and charge transfer impedance. The average electron transfer number and hydrogen peroxide calculated from RRDE are about 3.87 and 6.71%, respectively. These results show that the synthesized Pt-Cu/C has excellent electrocatalytic activity and the ORR is a four-electron dominant reduction pathway.

Keywords: Cyclic voltammetry · Pt-Cu alloy · Oxygen reduction reaction · Electrocatalyst

1. INTRODUCTION

Global problems related with the lack of sustainable and renewable energy sources as well as environmental pollution caused by fossil fuels are increasingly serious, fuel cells have long been considered to be a prospective solution to address these problems because of its ability to generate electricity from fuels such as hydrogen [1]. Oxygen reduction reaction (ORR) plays a key role in many reactions, such as electrocatalysis, electrochemical energy conversion/storage and metal corrosion, especially fuel cells [2-6]. Many organic and inorganic materials adhered on the electrode surface have

been fabricated as ORR catalysts, especially Pt nanoparticles [7]. Pt nanoparticles have long been considered as the most popular and the best efficient catalysts for the ORR and are still commonly applied in fuel cells [8-9]. Compared with other commercial catalysts, Pt based catalysts have low overpotential and high current density in a certain degree. Many forms of Pt have been prepared, such as highly ordered Pt nanotube arrays [10-12], mesoporous Pt [13], three-dimensional dendritic Pt nanostructures [14], Pt_n clusters [15]. However, Pt catalysts possess many other drawbacks, such as susceptibility to fuel crossover from the anode, low resistance to CO and methanol, and poor stability under electrochemical conditions [16]. In addition, the high cost and scarcity of Pt have been considered as the obstacles to apply for commercial fuel cells [17]. Hence, in view of activity and durability, great efforts such as reducing Pt loading or preparing nonoble metal even metal-free species have been made to research the advanced ORR catalysts to substitute the commercial Pt/C catalyst [18]. Alloying has been tended to be a promising approach to produce advanced catalytic materials [19]. Previous work have demonstrated that the bimetallic Pt-M catalysts where M represents a noble metal such as Ag, Ru, Au and Pd [20-21], or a transition metal such as Co, Ni, Cr, Mn, Zn, Fe, Cu [22-30] is not only reducing the content of Pt, but also enhancing the resistance of CO and methanol. Long et al. have successfully investigated the morphology, kinetics mechanism and catalytic activity of Pt-Pd alloy using a modified polyol method [31]. Zhu et al. synthesized a new class of 20 nm×2 nm ternary alloy FePtM (M=Cu, Ni) nanorods (NRs) which exhibited great improved ORR activity and durability by thermal decomposition [32]. These reports showed that modification is essential to reduce the content of Pt and improve the performance of the catalysts.

Nanoparticles synthesized as electrocatalyst by various methods, for example, wet chemical methods [33], need to be attached to a conductive support material and get connected to a charge collector which requires additional process steps fabricating the electrode [34, 35]. While, CV is a facile electrodeposition to adhere nanoparticles on a conductive substrate within only one step. CV has been an efficient method for synthesizing metal nanoparticles. Darko et al. have synthesized copper nanoparticles successfully by CV [36]. Arne et al. have designed highly porous platinum-based electrodes based on alternation of co-deposition and dealloying by CV for applying to glucose fuel cells [37]. Electrodeposition of Sn-Ag-Cu by CV and chronoamperometry was compared by Zhang et al [38].

Here, we reported the preparation of Pt-Cu nanoparticles supported on carbon (Pt-Cu/C) in situ CV method. Both physical morphologic characterization and electrochemical techniques were applied in our experiments. Scanning electron microscopy (SEM) was used to study the morphology of the nanoparticles. X-ray photoelectron spectroscopy (XPS) was performed to confirm the surface chemical composition and the metallic state. Electrochemical measurements of CV, rotating disk electrode (RDE), rotating ring disk electrode (RRDE) and electrochemical impedance spectroscopy (EIS) were used to study the electrocatalytic activity of the catalysts for ORR. The kinetics parameters of the ORR pathways were analyzed based on the obtained data which measured in various potential regions.

Our study highlights an efficient and simple method to synthesis a high performance electrocatalyst. This method may provide a new approach to synthesis the bimetallic Pt-M nanocatalyst, which could be expected to have applications in oxygen reduction reactions.

2. EXPERIMENTAL

2.1. Reagents and materials

Vulcan XC-72 carbon (Cabot, BET surface area of 235 $m^2 g^{-1}$), isopropanol (Aladdin, AR), nafion solution (Aldrich, 5 wt%), $HClO_4$ (Aladdin, AR, 70.0-72.0%), NaH_2PO_4 (J&K, AR), Na_2HPO_4 (J&K, AR), $CuSO_4$ (J&K, AR), $H_2PtCl_6 \cdot 6H_2O$ (Aladdin, AR), $K_3[Fe(CN)_6]$ (J&K, AR), $K_4[Fe(CN)_6] \cdot 6H_2O$ (J&K, AR), KCl (J&K, AR), KOH (J&K, AR) were used as received without any further purification. Pure grade O_2 or N_2 was used for saturating the solutions which were prepared with ultrapure water. The typical suspension of carbon was achieved as follows: 1.6 mg of the carbon blacks, 177 μL of isopropanol, 570 μL of ultra-pure water and 3 μL of nafion solution (Aldrich, 5 wt%) were mixed by ultrasonic in an ultrasonic bath (KQ-600KDE, 600 W) for 30 minutes.

2.2. Electrode preparations

The glassy carbon electrode was well polished with alumina suspension (0.3 μm), then rinsed thoroughly with ethanol and water in an ultrasonic bath to remove any alumina residues to get a mirror plane. And then, 8.5 μL of ink suspension was quantitatively transferred to a glassy carbon electrode and left to dry at room temperature, the obtained electrode was designated to C electrode. The C electrode was immersed in a mixed aqueous solution of 1 mM of $CuSO_4$ and 1 mM H_2PtCl_6, and cyclic voltammetry was conducted for 20 cycles in the range from -0.8 to 0.5 V *vs*. Ag/AgCl at a scan rate of 100 mV s^{-1} to fabricate the Pt-Cu/C electrode. The platinum modified electrode (Pt/C electrode) and copper modified electrode (Cu/C electrode) were obtained by using the same way as fabricating the Pt-Cu/C electrode without adding $CuSO_4$ or H_2PtCl_6.

2.3. Physical characterizations and electrochemical testing

A field-emission scanning electron microscopy (SEM, Hitachi, S-4800) with an accelerating voltage of 3 kV was used to observe the morphology of the samples. The surface chemical composition of the Pt-Cu/C and metallic state was recorded on Thermal Scientific ESCALAB 250Xi X-ray photoelectron spectroscopy with a monochromatic Al K_α (1486.6 eV) X-ray source and samples were measured under an ultrahigh vacuum ($<10^{-9}$ mbar). The high resolution survey scans were performed at a pass energy of 30 eV with a step size of 0.1 eV and all binding energies were calibrated using the C 1s carbon peak (284.6 eV). The XPS curves were fitted with a mixed Gaussian/Lorentzian fitting using the XPS peak fit 4.1 software, and a baseline fitting was conducted with a polynomial multi-point fitting carried out with the same software.

A conventional three-electrode system was performed to characterize the electrocatalytic activities of the samples in a 0.1 M KOH aqueous solution. The working electrode was a glassy carbon electrode (5 mm diameter, 0.196 cm^2). A Platinum foil and Ag/AgCl/sat. KCl electrode (0.197 V+0.0591×pH vs. RHE at 25 °C) were served as the counter and reference electrode, respectively. Before each measurement, the solution was originally purged with high-purity N_2 or O_2 for about 30

minutes and the gas was allowed to flow above the solution. Before electrochemical characterization, 20 cycles of potential cycling from -0.8 to 0.5 V at a scan rate of 100 mV s^{-1} were applied to activate the working electrode. Electrochemical measurements including CV, RDE, RRDE and EIS were carried out by an Autolab potentiostat/galvanostat (PGSTAT302N) with rotation control (AFMSRCE, Pine Instruments).

3. RESULTS AND DISCUSSION

3.1 Physical characterizations

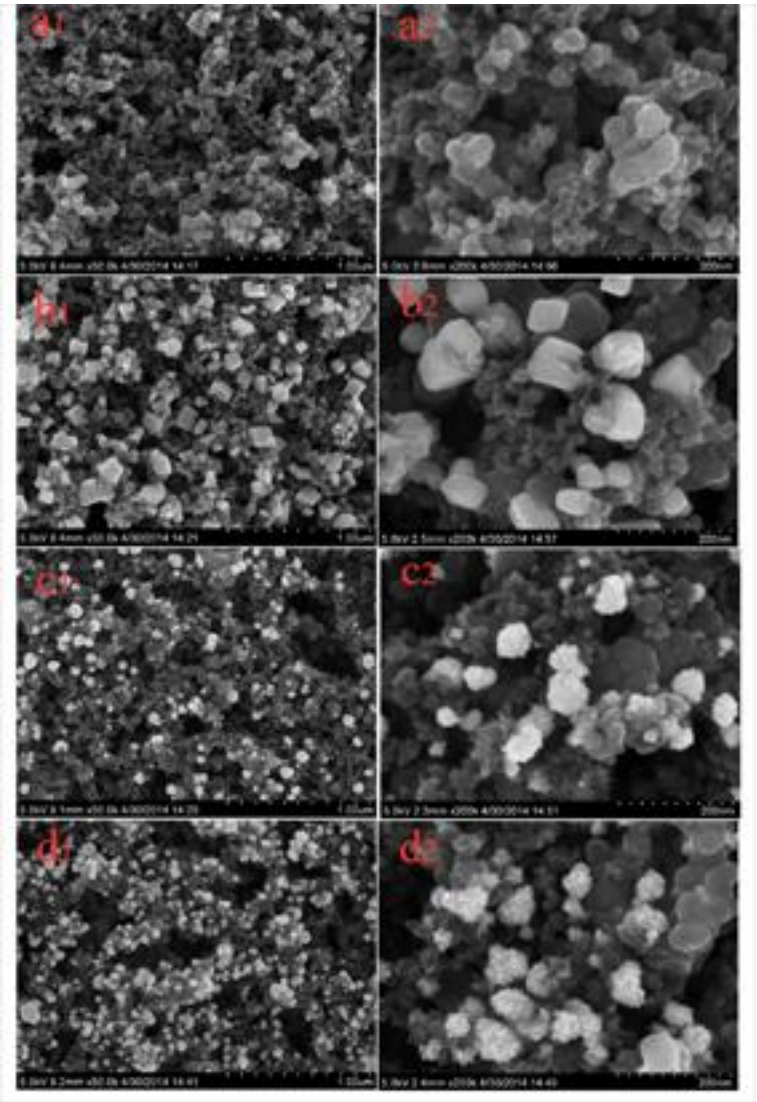

Figure 1. a, b, c, d Typical SEM images of C, Cu/C, Pt/C and Pt-Cu/C, respectively.

The nanoparticles of Cu, Pt and Pt-Cu alloy were electrochemically deposited on the surface of the carbon modified electrode by CV. Figure1 a-d show the typical SEM images of C, Cu, Pt, and Pt-Cu nanostructures. The SEM images reveal that the nanoparticles were firmly attached to the carbon surface with numerous internal pores. The deposited Cu nanoparticles have a cubic structure with the

size of about 70-110 nm (b_2). When the reaction was carried out in the presence of H_2PtCl_6, the resulted Pt-Cu nanoparticles have a flowerlike structure with a size of about 50-70 nm (d_2). When the reaction occurs in the presence of only H_2PtCl_6, the prepared Pt nanoparticles also have a flowerlike shape with an average size of 30-50 nm (c_2), a little smaller than that of Pt-Cu. It may be the case that the Pt nanoparticle grows outside the Cu nucleations to form the Pt-Cu alloy. Moreover, This porous structure of the Pt-Cu/C catalyst may facilitate the movement of oxygen into and out of the catalyst during the reduction reaction of oxygen, which plays the most key role on its electrocatalytic activity for ORR.

XPS was used to confirm the surface chemical composition of the Pt-Cu/C and metallic state. Distinct Pt 4f and Cu 2p peaks were displayed in Fig. 2, indicating the successfully incorporation of Pt and Cu. The $4f_{7/2}$ and $4f_{5/2}$ doublets of pure Pt sample locate at 70.9 and 74.2 eV were reported in previous studies [39]. However, as shown in Fig. 2a, there is a small increase in Pt binding energies as the $4f_{7/2}$ and $4f_{5/2}$ doublets of Pt locate at 71.6 and 75.4 eV, respectively, which has also been observed in Pt-Bi and Pt-Pb reported previously [40, 41]. The increase in the binding energies of Pt indicates the presence of a certain degree of interactions of copper with the Pt surface. Deconvolution of the Cu 2p region shows the presence of two pairs of doublets in Fig. 2b. The most intense doublet with binding energies of 932 eV (Cu $2p_{3/2}$) and 952 eV (Cu $2p_{1/2}$) is assigned to metallic Cu. Peaks at 932.4 eV (Cu $2p_{3/2}$) and 952.5 eV (Cu $2p_{1/2}$) could be attributed to Cu (I). Cu is predominant in metallic state of Pt-Cu/C. It may facilitate the increase of Pt nanoparticle size, because the presence of Cu may weaken the interaction between Pt and support, leading to a lower resistance to surface migration of Pt particles [42]. These results are highly consistent with above SEM observations (Fig. 1).

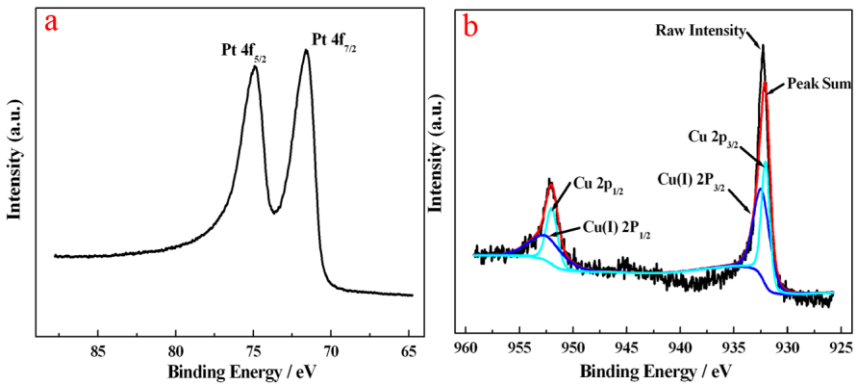

Figure 2. a, b XPS spectrum of Pt 4f, Cu 2p, respectively.

3.2 Electrochemical measurements

Characteristic CV was firstly applied to evaluate the electrocatalytic behaviors of Pt-Cu/C catalyst in O_2-saturated 0.1 M $HClO_4$, KOH, phosphate buffer solution (PBS, pH=7.06), with the aim to select the optimal electrolyte. As it is displayed in Fig. 3a, b, c, an obvious ORR peak corresponding to reduction of oxygen can be observed in each case, in KOH solution, Pt-Cu/C exhibits the highest ORR peak potential of 0.76 V, which is positive than that tested in PBS (0.6 V) and $HClO_4$ (0.62 V),

so, 0.1 M KOH aqueous solution is more preferred. Technique of Linear sweep voltammetry (LSV) was also used to confirm the CV result, as shown in Fig. 3e, d, f. Both the onset ORR potential and limiting current density characterized in 0.1 M KOH is the highest compared with those obtained from 0.1 M PBS and $HClO_4$, the data was clearly dedicated in Table 1. As a result, 0.1 M KOH aqueous solution was chosen as the optimal media to study the electrochemical activity of Pt-Cu/C since the minor positive shift in ORR potential, the onset ORR potential and the enhancement in current density toward ORR.

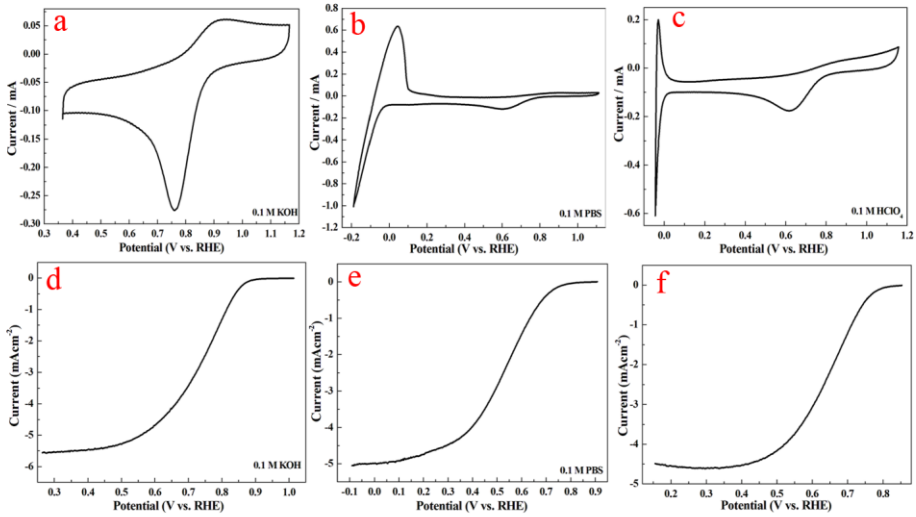

Figure 3. a, b, c CV of Pt-Cu/C in O_2-saturated 0.1 M KOH, PBS, $HClO_4$ at a scan rate of 100 mV s^{-1}. e, d, f ORR polarization curves of Pt-Cu/C in O_2-saturated 0.1 M KOH, PBS, $HClO_4$ with a scan rate of 10 mV s^{-1} at 1600 rpm.

Table 1. Comparison of electrochemical data for Pt-Cu/C electrode in 0.1 M KOH, PBS, $HClO_4$ solution.

	E_{ORR} (V vs. RHE)	E_{onset} (V vs. RHE)	$I_{limiting}$ (mA/cm^2)
KOH	0.764	0.864	-5.56
PBS	0.6	0.77	-5.05
$HClO_4$	0.6161	0.8261	-4.48

CV is also a traditional method to characterize the catalytic activity of catalysts with the ORR peak potential where the maximum oxygen reduction current occurs. The higher the ORR peak potential, the higher the catalytic activity. CV of Pt-Cu/C, Pt/C, Cu/C and C were carried out in N_2 and O_2 saturated 0.1 M KOH aqueous solution from 0.37 to 1.17 V vs. RHE. As shown in Fig. 4, Compared to the CV in the N_2-saturated KOH solution, the CV in the O_2-saturated solution exhibits

much larger anodic and cathodic current densities in each case. Which indicates that the as-synthesized catalysts display sensitive responses for the electrochemical behavior of O_2. It could also be found that the ORR peak potential varies greatly with immobilizing different metal nanoparticles indicating variable catalytic activities. An obvious ORR peak at around 0.76 V attributed to oxygen reduction of Pt-Cu/C can be observed, which shifts more positive than that of Pt/C (0.61 V), Cu/C (0.58 V) and C (0.56 V), as shown in Table 2. Furthermore, Pt-Cu/C exhibits the highest peak current density, indicating the Pt-Cu/C possesses the best electrocatalytic activity. According to the above phenomena, it is convincing that Pt-Cu/C is a good electrocatalyst, not only the content of Pt was reduced, but also the electrocatalytic activity was enhanced greatly.

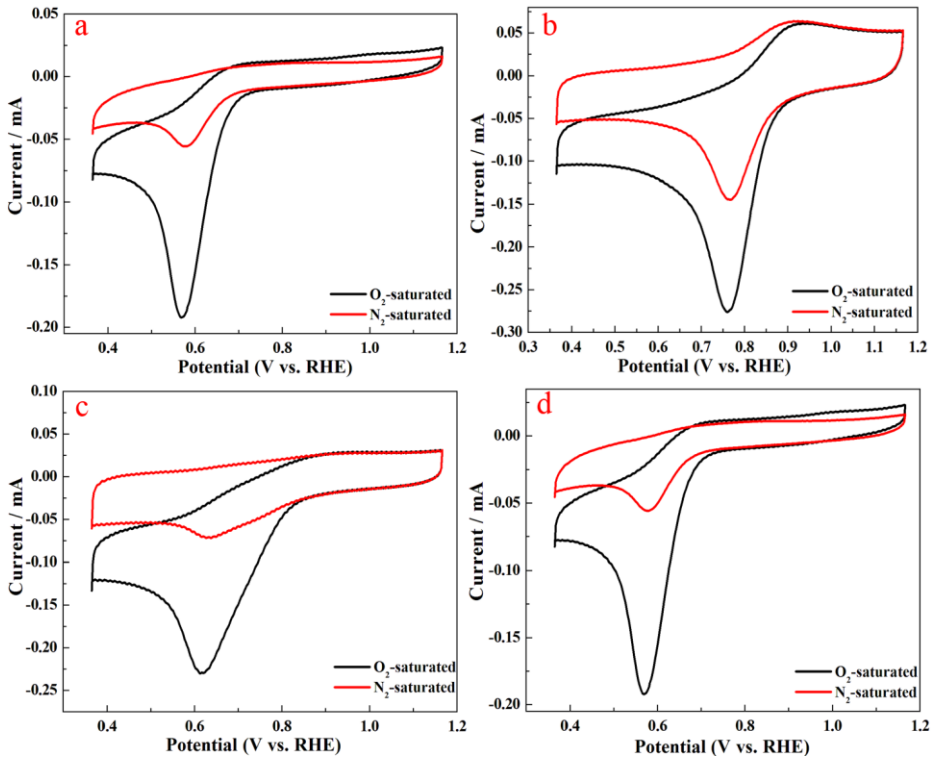

Figure 4. CV of Pt-Cu/C, Pt-C, Cu/C and C in O_2-saturated 0.1 M KOH at a scan rate of 100 mV s^{-1} from 0.37 to 1.17 V.

Table 2. Comparison of electrochemical data for different electrodes.

	E_{peak} (V vs. RHE)	E_{onset}	$I_{limiting}$ (mA/cm^2)	Average *n* (K-L)	Average *n* (RRDE)	Average %H_2O_2	Ref.
Pt-Cu/C	0.76	0.86	-5.56	3.93	3.87	6.27	
Pt/C	0.61	0.78	-4.34	2.97	2.82	59.24	
Cu/C	0.58	0.74	-3.26	2.43	2.47	76.83	
C	0.56	0.66	-2.42	1.93	-	-	
Pt-Cu/PPy	-	0.75	3.5	-	-	-	[47]
$PdNi_3$/C	0.85	0.995	5.2	-	-	-	[48]
Pt-Pd/PPVK	0.55	-	-	-	-	-	[49]

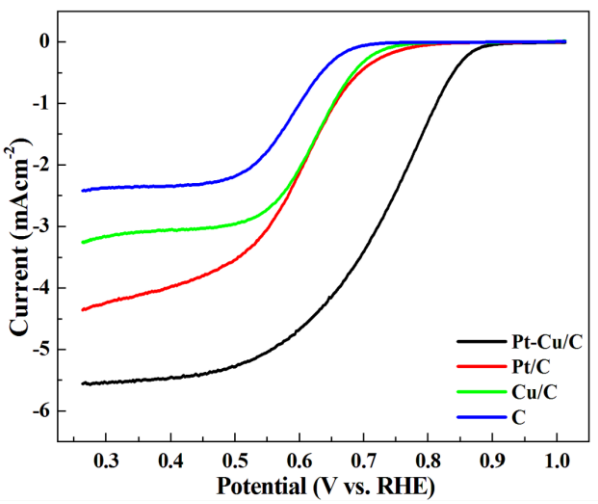

Figure 5. a ORR polarization curves with a scan rate of 10 mV s^{-1} and a rotation rate of 1600rpm for Pt-Cu/C, Pt-C, Cu/C and C in O_2-saturated 0.1 M KOH solution.

RDE measurement was applied to investigate the electrochemical properties of the catalysts, linear sweep curves of Pt-Cu/C, Pt/C, and Cu/C with a rotational rate of 1600 rpm in O_2-saturated 0.1 M KOH aqueous solution at a scan rate of 10 mV s^{-1} were shown in Fig. 5. A diffusion-limiting current region and the mixed kinetic-diffusion current region can be clearly observed from the polarization curves of the catalysts. For the Pt-Cu/C catalyst, the diffusion-limiting current region is under 0.54 V and the mixed kinetic-diffusion current region is between 0.54 V to 0.86 V. The Pt-Cu/C catalyst has the highest value of 5.56 mA cm^{-2} in limiting current density, which was followed by Pt/C (4.34 mA cm^{-2}), Cu/C (3.26 mA cm^{-2}) and C (2.42 mA cm^{-2}). And, in terms of the onset ORR potential, Pt-Cu/C (0.86 V vs. RHE) shifts more positive compared with that of Pt/C (0.78 V), Cu/C (0.74 V) and C (0.66 V) as shown in Table 2. The above results indicate that the Pt-Cu/C exhibits the best ORR electrocatalytic activities. What's more, the ORR polarization curves of these four catalysts were undertaken with various rotation rates and be used to give a deep insight into the electron transfer kinetics mechanisms, the data are shown in Fig. 6. As expected, the onset ORR potential of each catalyst is kept almost constant with all rotation rates and the current densities increased with the increasing of rotation speeds, which can be attributed to the more rapid oxygen diffusion on the electrode surface. The corresponding ORR performance in the diffusion and kinetically limited regions can be evaluated by Koutecky-Levich (K-L) plots which were generally used to calculate the electron number (*n*). The K-L equation was shown as below [43]:

$$\frac{1}{J}=\frac{1}{J_k}+\frac{1}{J_{\text{diff}}}=\frac{1}{J_k}+\frac{1}{B\omega^{1/2}} \qquad (1)$$

in which

$$B=\frac{0.62nFC_0D_0^{2/3}}{\eta^{1/6}} \qquad (2)$$

where J_k is the kinetic current density and J_{diff} the diffusion-limiting current density, ω is the angular velocity of the disk, n is the overall number of electrons transferred, F is the Faraday constant

(F=96485 C mol^{-1}), D_0 is the diffusion coefficient of O_2 in the electrolyte (in acidic media D_0=1.4×10^{-5} cm^2 s^{-1}, for pH=7-13 D_0=1.9×10^{-5} cm^2 s^{-1}), C_0 is the O_2 concentration in the electrolyte (for acidic media C_{O2}=1.1×10^{-3} mol L^{-1}, for pH=7-13 C_{O2}=1.2×10^{-3} mol L^{-1}), and η is the viscosity of the electrolyte (1.00×10^{-2} cm^2 s^{-1}) [44].

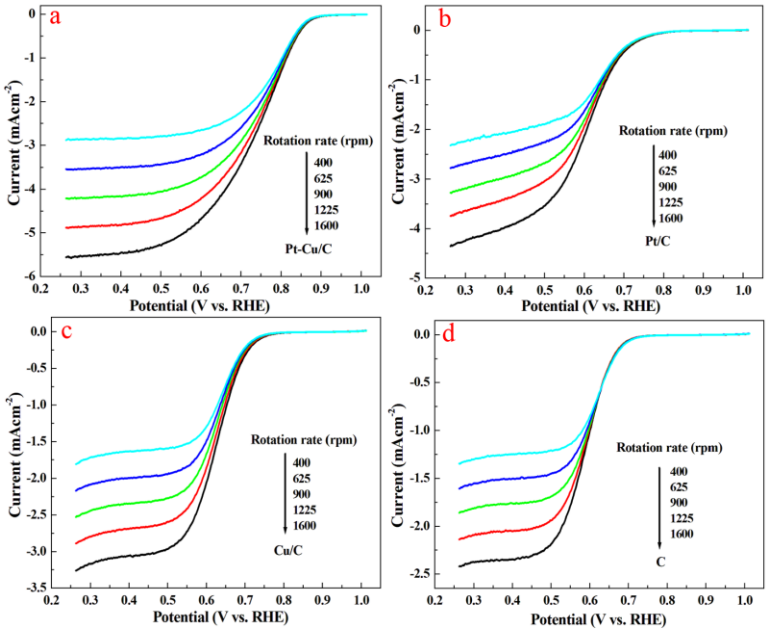

Figure 6. a, b, c, d RRDE polarization curves of Pt-Cu/C, Pt/C, Cu/C and C with various rotation rates in O_2-saturated 0.1 M KOH solution at scan rate of 10 mV s^{-1}.

ORR occurs either a direct four-electron reduction pathway where O_2 is reduced to H_2O or a two-electron reduction pathway where it is reduced to hydrogen peroxide (H_2O_2). In fuel cell processes, the four-electron direct pathway is more preferred and favorable [45].

As shown in Fig 7, the K-L plots show a good linearity between J^{-1} and $\omega^{-1/2}$ at various applied potentials, indicating the electron transfer for ORR is almost the same at various potentials [46]. And, the average electron transfer numbers are 3.93, 2.97, 2.46 and 1.93 for Pt-Cu/C, Pt/C, Cu/C and C, respectively, which was shown in Table 2. These results indicate the different ORR mechanisms among four catalysts. More specifically, Pt-Cu/C adopts a four-electron reaction pathway, while Pt/C and Cu/C takes a coexisting pathway involving both the two-electron and four-electron transfers, pure carbon black employs a two-electron reduction pathway. Moreover, Compared with the results of other research group [47, 48, 49] shown in Table 2, our results are may not so comparable and satisfactory, while the method of catalyst preparation was optimized to be more easier, and the electrocatalyst also are high efficient. In this sense, cyclic voltammetry for synthesizing Pt-Cu/C catalyst is adoptable. To further verify the results obtained from the K-L plots, RRDE technique was applied to evaluate the yield of H_2O_2 produced at the disk electrode and calculate the electron transfer number. RRDE polarization curves of Pt-Cu/C, Pt/C and Cu/C with various rotation rates were displayed in Fig. 8.

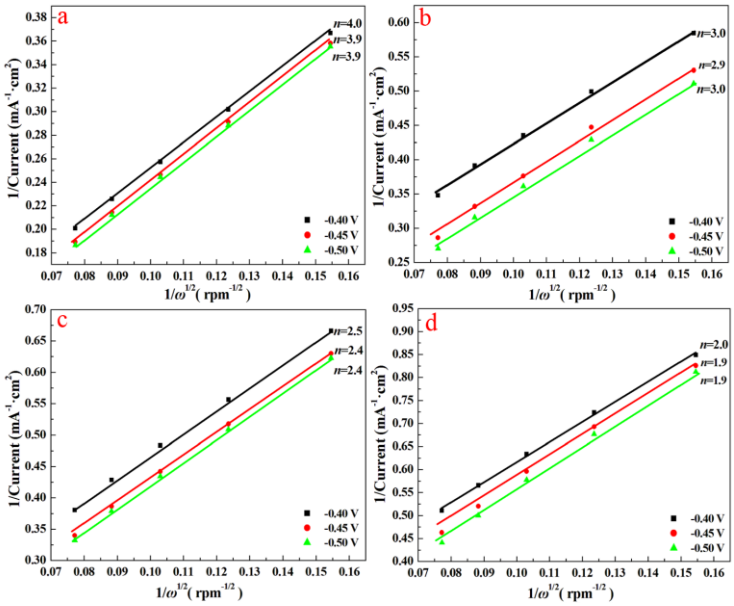

Figure 7. a, b, c, d K-L plots of Pt-Cu/C, Pt/C, Cu/C and C and the corresponding electron transfer number at various potentials.

In which, the lower part stands for the current-potential produced at the disk electrode when the O_2 was reduced, the upper part displays the current of ring electrode which was setted at 0.6 V to detect the formation of H_2O_2. The electron transfer number (n) and hydrogen peroxide yield ($\%H_2O_2$) can be obtained from the following equations [50]:

$$n = \frac{4i_d}{i_d + (i_r / N)} \qquad (3)$$

$$\%H_2O_2 = \frac{200i_r / N}{i_d + (i_r / N)} \qquad (4)$$

Where i_r and i_d are ring and disk currents, respectively, N is the ring collection efficiency that was tended to be 0.37 according to the instruction book.

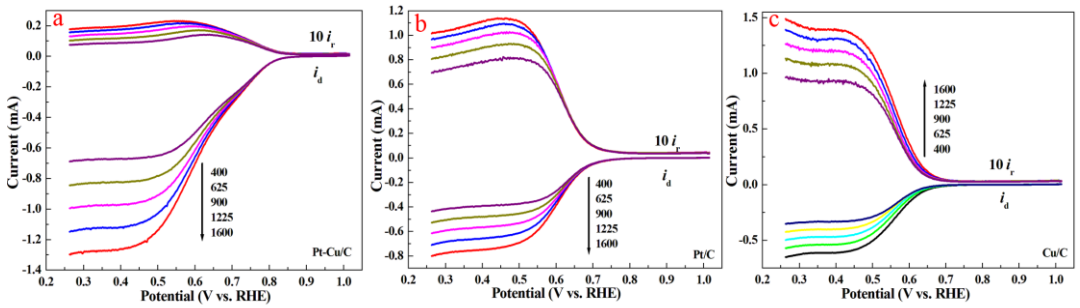

Figure 8. a, b, c RRDE polarization curves of Pt-Cu/C, Pt/C and Cu/C electrodes. Medium: O_2-saturated 0.1 M KOH aqueous solution, scan rate: 10 mV s^{-1}; ring potential: 0.6 V, and rotation rate: 400-1600rpm.

The H_2O_2 production and the electron numbers for Pt-Cu/C, Pt/C and Cu/C catalysts were shown in Fig.9, as seen from it, Pt-Cu/C has the lowest average H_2O_2 production of 6.71% which is much smaller than those of Pt/C (59.23%) and Cu/C (76.63%). Furthermore, the inverse order was occurred in the average electron transfer number, the average *n* for Pt-Cu/C is about 3.87, while the average *n* for Pt/C and Cu/C are 2.82 and 2.47 (Table 2), respectively. In addition, Fig. 10 displays the decreasing $\%H_2O_2$ with the increasing rotation rate, which is in line with the more rapid oxygen diffusion on the electrode surface during the RRDE measurement. In a word, all the results of RRDE are highly consistent with the results obtained from CV and ORR measurements mentioned above and the excellent electrocatalytic activity of Pt-Cu/C may be attributed to special structure of Pt-Cu alloy.

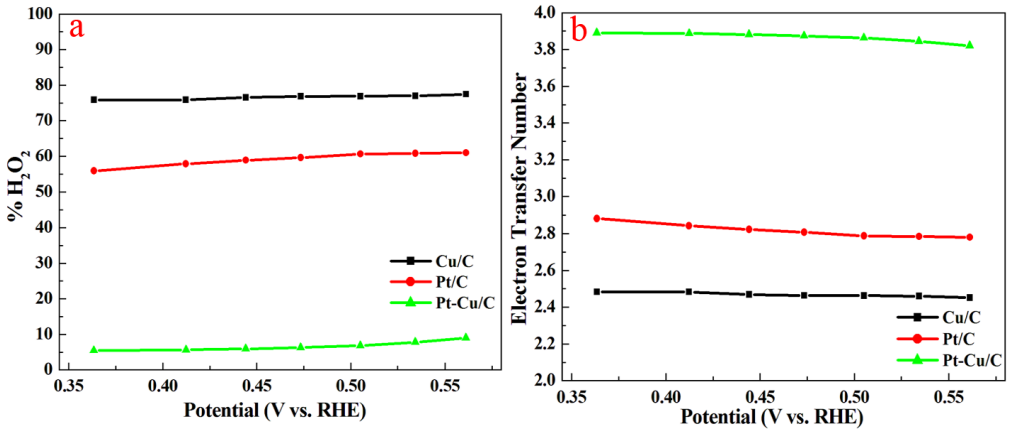

Figure 9. a, b The yield of H_2O_2 and the electron transfer number of Pt-Cu/C, Pt/C and Cu/C calculated from RRDE curves.

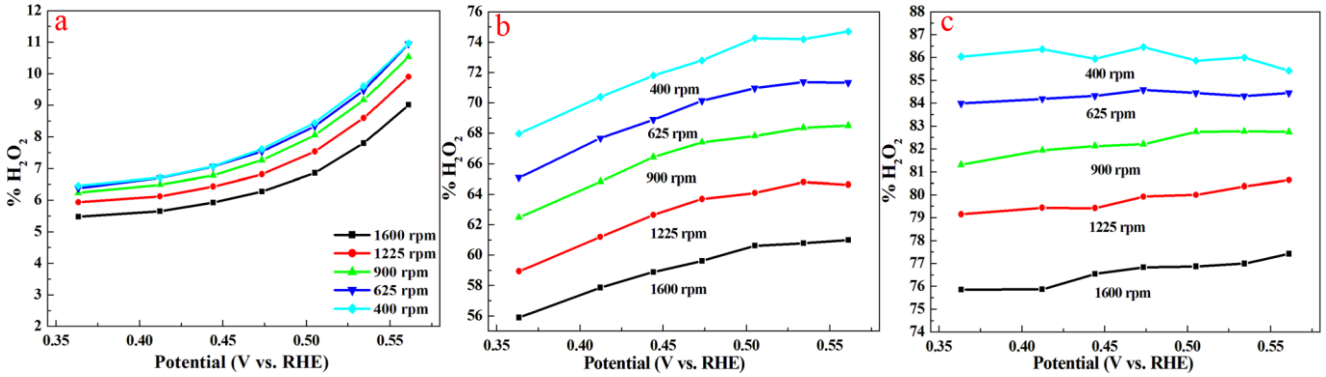

Figure 10. a, b, c The yield of H_2O_2 of Pt-Cu/C, Pt/C and Cu/C produced at disk electrode with the rotation from 400 rpm to 1600 rpm in 0.1 M KOH aqueous solution at scan rate of 10 mV s^{-1}.

The conductivity of the catalysts were tested by EIS which was performed in 0.1 M KCl solution containing 1.0 mM $K_3Fe(CN)_6$ and 1.0 mM $K_4Fe(CN)_6$ at 1.2 V in a frequency range of 0.1-100000 Hz. As clearly shown in Fig. 11, in spite of the similar shape of the impedance diagrams, there is an obvious difference between the diameters of the four semi-circles. That is, the diameters of the semicircles vary greatly with depositing different kinds of nanoparticles and the diameter of the

impedance arc (DIA) of Pt-Cu/C is much smaller than that of C, Cu/C and Pt/C, indicating smaller charge transfer impedance (R_p) on Pt-Cu/C electrode.

For getting more knowledge about the analysis, the equivalent circuit was used to fit the EIS data based on the above impedance results. The equivalent circuit including the elements of R_s, R_p, *CPE* and *W*. The interception of the arc with the real axis at the highest frequency was recorded by R_s is the solution impedance which is not of too much concern in this case. R_p is the charge transfer impedance directly measured by the semicircle diameter and it is the only circuit element that has a simple physical meaning describing how fast the rate of charge transfer is during oxidation reaction. Moreover, the lower charge transfer resistances usually have good correlations with the higher electrocatalytic activities of the catalysts [51]. A constant phase element (*CPE*) is related with double layer charge capacitance and adsorption of ions which may be due to the inhomogeneous surface of the electrode [52]. A warburg impedance (*W*) is associated with an infinite diffusion of ions through the interface between the electrolyte and the surface of the catalyst. By comparing the data in Table 3, Pt-Cu/C exhibits remarkably the lowest values of R_p (about 436 Ω calculated by the instrument) compared with those of Pt/C (565 Ω), Cu/C (1230 Ω) and C (2070 Ω), which suggesting Pt-Cu/C catalyst with a flowerlike structure has the best conductivity, and which may lead to the fastest electron transport. These results are in accordance with the CV, RDE, RRDE data, indicating that the flowerlike Pt-Cu/C is an excellent electrocatalyst.

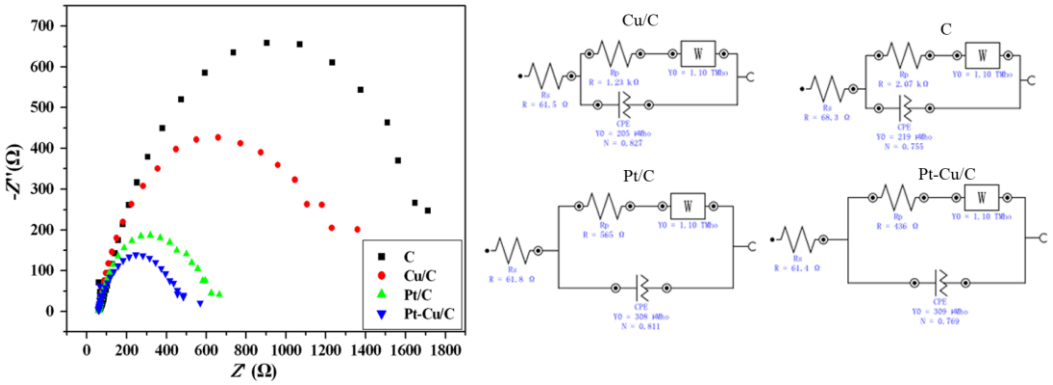

Figure 11. EIS plots of C, Cu/C, Pt/C, Pt-Cu/C electrode in 0.1 M KCl solution containing 1.0 mM $K_3Fe(CN)_6$ and 1.0 mM $K_4Fe(CN)_6$ at 1.2 V in a frequency range of 0.1-100000 Hz and the corresponding equivalent circuit.

Table 3. Values of elements in the equivalent circuits.

	R_S (Ω)	R_P (Ω)	*CPE* (μMHo)	*W* (TMho)
Pt-Cu/C	61.4	436	309	1.10
Pt/C	61.8	565	308	1.10
Cu/C	61.5	1230	205	1.10
C	68.3	2070	219	1.10

4. CONCLUSIONS

In this study, an electrochemical approach of CV has been performed for the synthesis of electrocatalysts for ORR. The Pt-Cu nanoparticles with a flowerlike structure were firmly attached to the carbon surface. Cu is predominant in metallic state of Pt-Cu/C, which may increase the size of Pt nanoparticle and increase the binding energies of Pt. What's more, compared with Cu/C and Pt/C, Pt-Cu/C exhibits the highest efficient catalytic activity towards ORR, as evidenced by the highest current density of the polarization curves, lowest onset oxidation potential and charge-transfer resistances. Moreover, the yields of H_2O_2 and *n* are 6.71% and 3.87 calculated from RRDE, which indicates Pt-Cu/C is a good catalyst with a four-electron reduction of oxygen. This catalyst may not be well-suited to wide application. Nevertheless, it is related with niche applications such as (micro) fuel cells, stimulation electrodes or electrochemical sensors.

ACKNOWLEDGEMENTS
The work was financially supported by the National Natural Science Foundation of China (31400044, 51473074), the General and Special Program of the postdoctoral science foundation China (2013M530397, 2014T70861), the Natural Science Foundation of Shandong province (ZR 2014JL009), and the Postgraduate Innovation Project of China university of petroleum (East China, YCX2014068).

References

1. E. Reddington, A. Sapienza, B. Gurau, R. Viswanathan, S. Sarangapani, E.S. Smotkin, T.E. Mallouk, *Science* 280 (1998) 1735.
2. V.S Murthi, R.C Urian, S. Mukerjee, *J. Phys. Chem. B*, 108 (2004) 11011.
3. B. Šljukić, C.E. Banks, R.G. Compton, *Phys. Chem. Chem. Phys*, 6 (2004) 4034.
4. I. Yagi, T. Ishida, K. Uosaki, *Electrochem. Commun*, 6 (2004) 773.
5. V. Soukharev, N. Mano, A. Heller, *J. Am. Chem. Soc*, 126 (2004) 8368.
6. H. Naohara, S. Ye, K. Uosaki, *Electrochim. Acta*, 45 (2000) 3305.
7. T. Selvaraju, R. Ramaraj, *Pramana-J Phys*, 65 (2005)713.
8. B. Lim, M. Jiang, P.H. Camargo, E.C. Cho, J. Tao, X. Lu, Y. Zhu, Y. Xia, *Science*, 324(2009)1302.
9. S. Wang, E. Iyyamperumal, A. Roy, Y. Xue, D. Yu, L. Dai, *Angew. Chem-Int. Edit*, 50 (2011) 11756.
10. J. Yuan, K. Wang, X. Xia, *Adv. Funct. Mater*, 15 (2005)803.
11. S. Hrapovic, Y. Liu, K.B. Male, J.H. Luong, *Anal. Chem*, 76(2004)1083.
12. H. Tang, J. Chen, S. Yao, L. Nie, G. Deng, Y. Kuang, *Anal. Biochem*, 331 (2004) 89.
13. S. Park, T.D. Chung, H.C. Kim, Nonenzymatic glucose detection using mesoporous platinum. *Anal. Chem*, 75 (2003) 3046.
14. Q. Shen, L. Jiang, H. Zhang, Q. Min, W. Hou, J-J. Zhu, *J. Phys. Chem. C*, 112(2008)16385.
15. S. Proch, M. Wirth, H.S. White, S. Anderson, J.Am. Chem. Soc, 135 (2013) 3073.
16. M. Winter, R.J. Brodd, *Chem. Rev.* 104 (2004) 4245.
17. A. Malheiro, J. Perez, H. Villullas, *J. Power. Sources*,195 (2010) 3111.
18. S. Chen, J. Bi, Y. Zhao, L. Yang, C. Zhang, Y. Ma, Q. Wu, X. Wang, Z. Hu, *Adv. Mater*, 24(2012) 5593.
19. C. Wang, D. Li, M. Chi, J. Pearson, R.B. Rankin, J. Greeley, Z. Duan, G. Wang, D. van der Vliet, K.L. More, N.M. Markovic, V.R. Stamenkovic, *J. Phys. Chem. Lett*, 3 (2012) 1668.

20. H. Zhang, Y. Yin, Y. Hu, C. Li, P. Wu, S. Wei, C. Cai, *J. Phys. Chem. C*, 114 (2010)11861.
21. Q. Yuan, Z. Zhou, J. Zhuang, X. Wang, *Chem. Commun*, 46 (2010) 1491.
22. Y. Zhang, Q. Huang, Z. Zou, J. Yang, W. Vogel, H. Yang, *J. Phys. Chem. C*, 114 (2010) 6860.
23. S. Guo, S. Dong, E. Wang, *J. Phys. Chem. C*, 113 (2009) 5485.
24. R. C. Venkateswara, B. Viswanathan, J. Phys. Chem. C, 113 (2009) 18907.
25. J. Kim, Y. Lee, S. Sun, *J. Am. Chem. Soc*, 132 (2010) 4996.
26. T.Y. Jeon, S.J. Yoo, Y.H. Cho, K.S. Lee, S.H. Kang, Y.E. Sung, *J. Phys. Chem. C*, 113 (2009) 19732.
27. C. Wang, D. van der Vliet, K.C. Chang, H. You, D. Strmcnik, J.A. Schlueter, N.M. Markovic, V.R. Stamenkovic, *J.Phys. Chem. C*, 113 (2009) 19365.
28. A. Sarkar, A. Manthiram, *J. Phys. Chem. C*, 114 (2010) 4725.
29. J. Wu, J. Zhang, Z. Peng, S. Yang, F.T. Wagner, H. Yang, *J. Am. Chem. Soc*, 132 (2010) 4984
30. A. Miura, H. Wang, B.M. Leonard, H.D. Abruna, F.J. DiSalvo, *Chem. Mater*, 21 (2009) 2661.
31. X. Cui, S. Wu, S. Jungwirth, Z. Chen, Z. Wang, L. Wang, Y. Li, Nano, 24 (2013) 295402.
32. H. Zhu, S. Zhang, S. Guo, D. Su, S. Sun, *J. Am. Chem. Soc*, 135 (2013) 7130.
33. Z. Peng, H. Yang, *Nano Today* 4 (2009) 143.
34. A. Kloke, F. von Stetten, R. Zengerle, S. Kerzenmacher, *Adv. Mater*, 23 (2011) 4976.
35. S. Litster, G. McLean, *J. Power. Sources*, 130 (2004) 61.
36. D. Grujicic, B.Pesic, *Electrochimi Acta* 47 (2002) 2901.
37. A. Kloke, C. Köhler, R. Gerwig, R. Zengerle, S. Kerzenmacher, *Adv. Mater*, 24 (2012) 2916.
38. J. Zhang, M. An, L. Chang, *Electrochimi. Acta*, 54 (2009) 2883.
39. J. Wang, P. Holt-Hindle, D. MacDonald, D.F. Thomas, A. Chen, *Electrochimi. Acta*, 53 (2008) 6944.
40. S. Kang, J. Lee, J.K. Lee, S.Y. Chung, Y. Tak, *J. Phys. Chem. B*, 110 (2006) 7270.
41. D. Blasini, D. Rochefort, E. Fachini, L. Alden, F. DiSalvo, C. Cabrera, H. Abruna, *Surf. Sci*, 600 (2006) 2670
42. M. Kang, Y.S. Bae, C.H. Lee, *Carbon*, 43 (2005) 1512.
43. Z. Chen, D. Higgins, Z. Chen, *Carbon*, 48 (2010) 3057.
44. I. Kocak, M.A. Ghanem, A. Al-Mayouf, M. Alhoshan, P.N. Bartlett, *J. Electronanal. Chem*, 706 (2013) 25.
45. M. Jahan, Q. Bao, K.P. Loh, *J. Am. Chem. Soc*, 134 (2012) 6707.
46. Y. Gochi-Ponce, G. Alonso-Nunez, N. Alonso-Vante, *Electrochem. Commun*, 8 (2006) 1487-1491
47. M. Saremi, M. Salehisaki, *Electroanal*, 26 (2014) 1606.
48. B. Li, J. Prakash, *Electrochem. Commun*, 11(2009) 1162.
49. F. Jiang, F. Ren, W. Zhou, Y. Du, J. Xu, P. Yang, *Fuel*, 102(2012) 560.
50. K. Lee, L. Zhang, H. Lui, R. Hui, Z.Shi, J. Zhang, *Electrochim. Acta*, 54 (2009) 4704.
51. H. Meng, P.K. Shen, *Electrochem. Commun*, 8 (2006) 588.
52. E. Yu, K. Scott, R. Reeve, *Fuel. Cells*, 3 (2003) 169.